JBMR®

FGF23 Regulates Bone Mineralization in a 1,25(OH)$_2$D$_3$ and Klotho-Independent Manner

Sathish Kumar Murali,[1] Paul Roschger,[2] Ute Zeitz,[1] Klaus Klaushofer,[2] Olena Andrukhova,[1] and Reinhold G Erben[1]

[1]Department of Biomedical Sciences, University of Veterinary Medicine, Vienna, Austria
[2]Ludwig Boltzmann Institute of Osteology at the Hanusch Hospital of WGKK and AUVA Trauma Center Meidling, 1st Medical Department, Hanusch Hospital, Vienna, Austria

ABSTRACT

Fibroblast growth factor-23 (Fgf23) is a bone-derived hormone, suppressing phosphate reabsorption and vitamin D hormone (1,25(OH)$_2$D$_3$) production in the kidney. It has long been an enigma why lack of Fgf23 or of Klotho, the coreceptor for Fgf23, leads to severe impairment in bone mineralization despite the presence of hypercalcemia and hyperphosphatemia. Using $Fgf23^{-/-}$ or $Klotho^{-/-}$ mice together with compound mutant mice lacking both $Fgf23$ or $Klotho$ and a functioning vitamin D receptor, we show that in $Klotho^{-/-}$ mice the mineralization defect is solely driven by 1,25(OH)$_2$D$_3$-induced upregulation of the mineralization-inhibiting molecules osteopontin and pyrophosphate in bone. In $Fgf23^{-/-}$ mice, the mineralization defect has two components, a 1,25(OH)$_2$D$_3$-driven component similar to $Klotho^{-/-}$ mice and a component driven by lack of Fgf23, causing additional accumulation of osteopontin. We found that FGF23 regulates osteopontin secretion indirectly by suppressing alkaline phosphatase transcription and phosphate production in osteoblastic cells, acting through FGF receptor-3 in a Klotho-independent manner. Hence, FGF23 secreted from osteocytes may form an autocrine/paracrine feedback loop for the local fine-tuning of bone mineralization. © 2015 American Society for Bone and Mineral Research.

KEY WORDS: FIBROBLAST GROWTH FACTOR-23 (FGF23); KLOTHO; VITAMIN D; BONE MINERALIZATION

Introduction

Fibroblast growth factor-23 (Fgf23) is a bone-derived phosphaturic hormone secreted by osteoblasts and osteocytes in response to phosphate and vitamin D.[1] Fgf23 suppresses reuptake of filtered phosphate and vitamin D hormone production in renal proximal tubules[2,3] and stimulates uptake of calcium and sodium in distal tubules.[4,5] Binding of Fgf23 to the ubiquitously expressed fibroblast growth factor receptor 1c (FGFR1c) requires the obligatory coreceptor α-Klotho (Klotho). The *Klotho* gene encodes for a type 1 transmembrane protein with homology to glycosidases.[6] Expression of Klotho is localized to a few tissues such as the proximal and distal tubules in kidney, choroid plexus, testis, and the sinoatrial node in the heart.[2,6] In addition, *Klotho* may also be expressed in bone.[7] Because Klotho-deficient mice are characterized by an aging-like phenotype,[6] Klotho was originally thought to be an anti-aging factor and was named after the Greek goddess spinning the thread of life. However, later studies showed that Klotho acts as a coreceptor for Fgf23, converting the ubiquitously expressed fibroblast growth FGFR1c into an Fgf23-specific receptor[8] and, thus, targeting the hormonal actions of Fgf23 to tissues expressing Klotho.

The aging-like phenotype in Klotho- and Fgf23-deficient mice is owing to intoxication with the vitamin D hormone[9–11] because the suppressive action of Fgf23 signaling is essential for the regulation of renal 1α-hydroxylase, the rate-limiting step in the vitamin activation pathway. Absence of Fgf23 or Klotho signaling in renal proximal tubules results in overexpression of 1α-hydroxylase, leading to excessive production of the vitamin D hormone (1,25(OH)$_2$D$_3$). Therefore, both Fgf23- and Klotho-deficient mice are characterized by profoundly increased circulating 1,25(OH)$_2$D$_3$ and subsequent hypercalcemia and hyperphosphatemia.[7,12]

In addition to the aging-like phenotype, Klotho- and Fgf23-deficient mice show impaired bone mineralization and osteomalacia,[7,12] which was initially interpreted as osteoporosis.[6] It has long been an enigma why bone mineralization is defective in Klotho$^{-/-}$ and Fgf23$^{-/-}$ mice despite the presence of hypercalcemia and hyperphosphatemia in these mice. Bone mineralization is a complex process restricted to bone tissue and teeth. The organic and inorganic constituents of the mineralization process are secreted by osteoblasts and osteocytes.[13] Several factors are involved in the regulation of the mineralization process during hydroxyapatite (HA) crystal formation and deposition of HA crystals in the extracellular matrix (ECM). Pyrophosphate (PPi), a

small diphosphate molecule secreted by osteoblasts during matrix mineralization, is a potent regulator of the mineralization process. PPi directly binds to the HA crystals, thereby inhibiting their growth and deposition onto collagen I. It is well established that increased levels of PPi in the ECM lead to impaired bone mineralization.[14,15] Conversely, absence of PPi in the ECM owing to targeted ablation of the PPi-transporter progressive ankylosis (ANK) leads to severe ectopic crystal deposition and joint fusion.[16] Another inhibitor of bone mineralization is the extracellular matrix protein osteopontin (OPN). Like PPi, OPN also has the ability to directly bind to HA crystals, thereby blocking its deposition onto collagen I.[17] In accordance with the inhibitory role of OPN on the mineralization process, $OPN^{-/-}$ mice display higher bone mineral content and mineral crystallinity than wild-type (WT) mice.[18] Furthermore, increased serum levels of OPN are associated with impaired bone mineralization.[7]

It has long been known that treatment of rats with high doses of the vitamin D hormone ($1,25(OH)_2D_3$) leads to impaired bone mineralization.[19,20] However, the mechanism underlying this effect has not been elucidated until recently. Lieben and colleagues[14] showed that $1,25(OH)_2D_3$ inhibits bone mineralization through increased osteoblastic expression of genes involved in the production and extracellular transportation of PPi, and also through increased expression of OPN. Because lack of *Klotho* and *Fgf23* leads to increased serum levels of $1,25(OH)_2D_3$,[12,21] we hypothesized that excessive $1,25(OH)_2D_3$ signaling in $Klotho^{-/-}$ and $Fgf23^{-/-}$ mice is responsible for the impairment in bone mineralization observed in these mice. To test our hypothesis, we ablated vitamin D signaling in $Klotho^{-/-}$ and $Fgf23^{-/-}$ mice by crossing them with mice expressing a nonfunctioning vitamin D receptor ($VDR^{\Delta/\Delta}$), thus generating $Klotho^{-/-}/VDR^{\Delta/\Delta}$ and $Fgf23^{-/-}/VDR^{\Delta/\Delta}$ compound mutants. All mice were kept lifelong on a so-called rescue diet, which has been shown to normalize calcium and phosphate homeostasis in VDR-ablated mice.[22] We previously showed that bone turnover and glucose homeostasis is normal in $Klotho^{-/-}/VDR^{\Delta/\Delta}$ and in $Fgf23^{-/-}/VDR^{\Delta/\Delta}$ compound mutant mice on rescue diet.[9,11] Here, we report that the bone mineralization defect in *Klotho*-deficient mice is caused by $1,25(OH)_2D_3$-driven upregulation of pyrophosphate and osteopontin in bone. In addition, we show that Fgf23 has a physiological role in bone mineralization, regulating OPN indirectly through transcriptional control of tissue nonspecific alkaline phosphatase (TNAP) in a vitamin D- and Klotho-independent manner.

Materials and Methods

Animals

All animal procedures were approved by the Ethical Committees of the University of Veterinary Medicine Vienna and of the local government authorities. Heterozygous $VDR^{+/\Delta}$ [1] were mated with heterozygous $Klotho^{+/-}$ (Lexicon Genetics, Mutant Mouse Regional Resource Centers, University of California, Davis, CA, USA) and $Fgf23^{+/-}$ [10] mutant mice to generate double heterozygous animals. $Klotho^{+/-}/VDR^{+/\Delta}$ and $Fgf23^{+/-}/VDR^{+/\Delta}$ mutant mice on C57BL/6 background were interbred to generate WT, $VDR^{\Delta/\Delta}$, $Klotho^{-/-}$, $Klotho^{-/-}/VDR^{\Delta/\Delta}$, $Fgf23^{-/-}$, and $Fgf23^{-/-}/VDR^{\Delta/\Delta}$ mutant mice. Genotyping of the mice was performed by multiplex PCR using genomic DNA extracted from tail as described.[9] The mice were kept at 24°C with a 12-hour light/dark cycle and were allowed free access to a rescue diet and tap water. The rescue diet (Sniff,

Soest, Germany) containing 2.0% calcium, 1.25% phosphorus, 20% lactose, and 600 IU vitamin D/kg was fed starting from age 16 days. This diet has been shown to normalize mineral homeostasis in VDR-ablated mice.[22,23] All experiments were performed on 4-week-old offspring of double heterozygous × double heterozygous mutants. At necropsy, the mice were exsanguinated from the abdominal V. cava under anesthesia with ketamine/xylazine (67/7 mg/kg ip) for serum collection.

Biochemical analyses

Serum calcium and phosphorus were analyzed using a Cobas c111 analyzer (Roche, Mannheim, Germany). Serum intact Fgf23 (Kainos, Tokyo, Japan), $1,25(OH)_2D$ (IDS, Boldon, UK), and intact PTH (Immutopics, San Clemente, CA, USA) were determined by ELISA.

RNA isolation and quantitative real-time PCR

Right femurs were collected, carefully defleshed, and shock-frozen in liquid nitrogen after flushing out the bone marrow. Shock-frozen tissues were homogenized in TRI Reagent (Molecular Research Center, Cincinnati, OH, USA), and total RNA was extracted according to the manufacturer's protocol. RNA purity and quality were determined using a 2100 Bioanalyzer (Agilent Technologies, Santa Clara, CA, USA). Two micrograms of RNA was used for first-strand cDNA synthesis (iScript cDNA Synthesis Kit, Bio-Rad, Hercules, CA, USA). Quantitative RT-PCR was performed on a Rotor-Gene 6000 (Qiagen, Valencia, CA, USA) using QuantiFast EverGreen PCR Kit (Qiagen). A melting curve analyses was performed for all assays. Primer sequences are given in Supplemental Table S1. Efficiencies were examined based on a standard curve. Expression of target genes was normalized to the expression of the housekeeping gene glyceraldehyde-3-phosphate-dehydrogenase (GAPDH).

Micro–computed tomography (µCT) analysis

Left femurs were collected and stored in 70% ethanol. Quantitative micro–computed tomography (µCT35, SCANCO Medical AG, Brüttisellen, Switzerland) was used to assess cortical and trabecular bone bone mineral density (BMD) as described previously, using a voxel size of 3.5 µm (isotropic). [24] The µCT measurements were performed in compliance with recently published guidelines.[25] BMD values were expressed as mg HA/ccm.

Quantitative backscattered electron imaging (qBEI)

Bone mineralization density distribution (BMDD) from the femoral cortical midshaft region was determined using qBEI, as previously described.[26] Distal femurs were fixed in 70% v/v ethanol, dehydrated in ethanol, and embedded in methylmethacrylate.[27] Plastic blocks with micro-ground and polished surfaces were prepared. A digital scanning electron microscope (DSM 962, Zeiss, Oberkochen, Germany) operated at an accelerating voltage of 20 kV, a probe current of 110 pA, and equipped with a four-quadrant semiconductor backscattered electron detector was used. Images with spatial resolution of 1 µm per pixel were acquired for BMDD measurements. The BMDD parameter CaMean, reflecting the weighted mean Ca concentration of the mineralized bone area, and CaLow, indicating the percentage of bone area with a calcium concentration of less than 17.68 weight%, were calculated.

Bone histology and histomorphometry

Isolated mouse femurs were fixed in 4% paraformaldehyde at 4°C overnight and were processed and embedded in methylmethacrylate as described previously.[27] Midsagittal sections of the distal femurs were prepared using a HM 355S microtome (Microm, Walldorf, Germany) and were stained with von Kossa/McNeal.[28] Histomorphometric measurements were made on sections stained with von Kossa/McNeal using a semiautomatic system (Osteomeasure, Osteometrics, Decatur, GA, USA) and a Zeiss Axioskop microscope (Carl Zeiss Microscopy, Jena, Germany) with a drawing attachment. Osteoid thickness (O.Th) and osteoid volume (OV/BV) were measured in cortical bone of the femoral midshaft and in cancellous bone of the distal femoral metaphysis at ×20 magnification. The area within 0.25 mm from the growth plate was excluded from histomorphometric cancellous bone measurements.

Osteoblast isolation and in vitro experiments

Calvariae were aseptically harvested from 3-day-old mice, minced, and incubated with digestion medium (α-MEM medium, 2 mg/mL type II collagenase (Invitrogen, Carlsbad, CA, USA) and 2% penicillin-streptomycin) at 37°C in a water bath for 4 hours. Bone fragments were washed with PBS and cultured in α-MEM medium supplemented with 2% penicillin-streptomycin and 10% calf serum (PAA/GE Healthcare, Piscataway, NJ, USA). After osteoblastic differentiation (50 μg/mL ascorbic acid and 10 mM β-glycerophosphate) for 6 days, cells were treated with 10^{-7} M or 10^{-8} M of 1,25(OH)$_2$D$_3$, 10 or 100 ng/mL of recombinant human FGF23 R176/179Q (rFGF23, kindly provided by Amgen Inc., Thousand Oaks, CA, USA), 20 ng/mL rat anti-FGF23 antibody (kindly provided by Amgen Inc.), 10 nM FGFR1 inhibitor PD173074 (Sigma, St. Louis, MO, USA), 120 nM pan FGFR inhibitor (FIIN1 hydrochloride, Tocris Bioscience, Bristol, UK), 5 ng/mL ERK inhibitor PD184352 (Sigma), and 25 nM FGFR3 inhibitor PD173074 (Sigma) for 24 hours. At various times after treatment, cell culture supernatant and samples for RNA isolation were collected and stored at −80°C.

Kidney distal tubular segment preparation

Renal distal tubular segments were isolated from C57BL/6 wild-type mice as previously described.[4] Distal tubular segments were incubated for 24 hours with vehicle or different doses of rFGF23. Thereafter, the segments were snap-frozen for RNA isolation.

Immunohistochemistry

For immunohistochemistry, 5-μm-thick undecalcified sections were obtained from plastic-embedded femurs as described.[27] Sections were deplastified, incubated for 15 minutes in 3% hydrogen peroxide in PBS to block endogenous peroxidase activity, and, after blocking with 10% rabbit serum, incubated with anti-OPN (Abcam, Cambridge, MA, USA; 1:300) at 4°C overnight. After washing, sections were incubated for 2 hours with biotinylated goat anti-rabbit secondary antibody (1:2000, Vector, Burlingame, CA, USA). Finally, the sections were counterstained with Mayer's hematoxylin. Negative control was performed by omitting primary antibody. The sections were analyzed using a Zeiss Axioskop 2 microscope.

Protein isolation from bone

Proteins from femurs were isolated using a previously described protocol.[29] Briefly, femurs were carefully defleshed and bone marrow was flushed out. After demineralizing (300 μL of 1.2 M HCl at 4°C overnight), proteins from the femur bones were isolated using 6M guanidine-HCL in 100 mM Tris buffer, pH 7.4, at 4°C for 72 hours. Extracted proteins were concentrated using ethanol precipitation and redissolved in 8 M urea buffer. Protein concentration was determined using a BCA assay (Thermo Scientific, Waltham, MA, USA).

Western blotting

Proteins were solubilized in Laemmli sample buffer, fractionated on SDS-PAGE (50 μg/well), and transferred to a nitrocellulose membrane (Thermo Scientific). Immunoblots were incubated overnight at 4°C with polyclonal rabbit anti-OPN (1:2000, Abcam) and monoclonal mouse anti-β-actin (1:5000, Sigma) in 2% (w/v) bovine serum albumin (BSA, Sigma) in a TBS-T buffer (150 mM NaCl, 10 mM Tris [pH 7.4/HCl], 0.2% [v/v] Tween-20). After washing, membranes were incubated with horseradish peroxidase-conjugated secondary antibodies (Amersham Life Sciences/GE Healthcare). Specific signal was visualized by ECL kit (Amersham Life Sciences/GE Healthcare). The protein bands were quantified by ImageQuant 5.0 software (Molecular Dynamics/GE Healthcare).

Quantification of PPi levels

After extracting PPi from whole femurs with 1.2 M HCl at 4°C overnight, evaporation of HCl at 99°C, and resuspension of the samples in deionized water, the amount of PPi was quantified using the PPiLight Inorganic Pyrophosphate Assay (Lonza, Walkersville, MD, USA) according to the manufacturer's protocol. Sodium pyrophosphate tetrabasic decahydrate (Sigma) was used as standard.

Statistical analysis

Statistics were computed using PASW Statistics 17.0 (SPSS Inc., Chicago, IL, USA). The data were analyzed by two-sided *t* test (2 groups) or 1-way analyses of variance (ANOVA) followed by Student-Newman-Keuls multiple comparison test (>2 groups). Any *p* values less than 0.05 were considered significant. Data represent mean values ± SEM.

Results

Ablation of vitamin D signaling rescues bone mineralization in Klotho$^{-/-}$/VDR$^{\Delta/\Delta}$ but not in Fgf23$^{-/-}$/VDR$^{\Delta/\Delta}$ compound mutants.

In accordance with previous reports,[9,11] 4-week-old VDR$^{\Delta/\Delta}$, Fgf23$^{-/-}$/VDR$^{\Delta/\Delta}$, and Klotho$^{-/-}$/VDR$^{\Delta/\Delta}$ mice on rescue diet were normocalcemic and normophosphatemic (Table 1), an important prerequisite for a study examining bone mineralization in these compound mutant mice. However, similar to our earlier studies in 4-week-old VDR mutant mice,[9,11] we found moderately elevated serum levels of parathyroid hormone (PTH) in 4-week-old VDR$^{\Delta/\Delta}$, Fgf23$^{-/-}$/VDR$^{\Delta/\Delta}$, and Klotho$^{-/-}$/VDR$^{\Delta/\Delta}$ mice on rescue diet, relative to wild-type mice (Table 1). It is possible that the rescue diet may not be able to fully correct serum PTH levels in young, fast-growing VDR$^{\Delta/\Delta}$ mice. It is well known that Klotho$^{-/-}$ and Fgf23$^{-/-}$ mice are characterized by

Table 1. Serum Clinical Chemistry and Renal mRNA Expression of Vitamin D-Metabolizing Enzymes

Variable	WT	VDR$^{\Delta/\Delta}$	Klotho$^{-/-}$	Klotho$^{-/-}$/ VDR$^{\Delta/\Delta}$	Fgf23$^{-/-}$	Fgf23$^{-/-}$/ VDR$^{\Delta/\Delta}$
Serum calcium (mmol/L)	2.35 ± 0.09	2.21 ± 0.16	3.02 ± 0.16[a,b]	2.28 ± 0.14	2.95 ± 0.15[a,b]	2.23 ± 0.12
Serum phosphorus (mmol/L)	3.85 ± 0.12	3.44 ± 0.17	5.18 ± 0.21[a,b]	3.38 ± 0.17	5.31 ± 0.18[a,b]	3.41 ± 0.14
Serum PTH (pg/mL)	10.5 ± 4	116 ± 8[a]	10 ± 4[b]	95 ± 5[a]	8 ± 3[b]	105 ± 11[a]
Serum 1,25(OH)$_2$D (pmol/L)	50 ± 21	321 ± 65[a]	458 ± 53[a]	269 ± 59[a]	489 ± 29[a]	286 ± 39[a]
Serum Fgf23 (pg/mL)	180 ± 16	210 ± 21	576 ± 32[a,b]	211 ± 19	n.d.	n.d.
Relative renal CYP27B1 mRNA expression	0.92 ± 0.09	3.86 ± 0.83[a]	6.28 ± 1.31[a]	5.87 ± 0.70[a]	6.18 ± 0.73[a]	6.51 ± 0.54[a]
Relative renal CYP24A1 mRNA expression	0.92 ± 0.22	0.15 ± 0.04[a]	0.91 ± 0.37	0.10 ± 0.03[a]	1.05 ± 0.35	0.25 ± 0.10[a]

n.d. = not detectable.
[a] $p < 0.05$ versus VDR$^{\Delta/\Delta}$ mice.
[b] $p < 0.05$ versus WT.

elevated serum levels of 1,25(OH)$_2$D because of the absence of the inhibitory effect of Fgf23 signaling on renal 1α-hydroxylase (CYP27B1) expression.[7,12,30] We also found distinctly increased circulating 1,25(OH)$_2$D in Klotho$^{-/-}$ and Fgf23$^{-/-}$ mice, relative to WT mice, in our experiment (Table 1). The increase in serum 1,25(OH)$_2$D in Klotho$^{-/-}$ and Fgf23$^{-/-}$ mice was associated with increased CYP27B1, but unchanged CYP24A1, mRNA expression in the kidney (Table 1). 24-hydroxylase (CYP24A1) is the most important enzyme initiating vitamin D degradation.[31] As a consequence of increased renal CYP27B1 and suppressed CYP24A1 mRNA expression, serum 1,25(OH)$_2$D was also elevated in VDR$^{\Delta/\Delta}$, Fgf23$^{-/-}$/VDR$^{\Delta/\Delta}$, and Klotho$^{-/-}$/VDR$^{\Delta/\Delta}$ mice lacking a functional VDR. This effect may be attributable to lacking 1,25(OH)$_2$D$_3$-mediated feedback inhibition,[32] and/or moderately elevated serum PTH in VDR mutant mice. In agreement with earlier reports,[12] serum intact Fgf23 was profoundly increased in Klotho$^{-/-}$ mice (Table 1). Interestingly, however, ablation of vitamin D signaling normalized serum intact Fgf23 in Klotho$^{-/-}$/VDR$^{\Delta/\Delta}$ compound mutants, indicating that the very high serum concentrations of intact Fgf23 found in Klotho$^{-/-}$ mice are because of 1,25(OH)$_2$D$_3$-driven upregulation of Fgf23 secretion (Table 1).

To initially examine bone mineralization in Fgf23$^{-/-}$/VDR$^{\Delta/\Delta}$ and Klotho$^{-/-}$/VDR$^{\Delta/\Delta}$ compound mutants, we performed μCT-based analyses of cortical BMD in the femoral midshaft of 4-week-old wild-type, VDR$^{\Delta/\Delta}$, Klotho$^{-/-}$, Fgf23$^{-/-}$, Fgf23$^{-/-}$/VDR$^{\Delta/\Delta}$, and Klotho$^{-/-}$/VDR$^{\Delta/\Delta}$ compound mutants on rescue diet. In accordance with previous studies,[7,9,11,12] we found decreased cortical and trabecular BMD (bone only without bone marrow) in femurs of Klotho$^{-/-}$ and Fgf23$^{-/-}$ mutants compared with WT and VDR$^{\Delta/\Delta}$ mice (Fig. 1A and Supplemental Fig. S1A). Ablation of vitamin D signaling completely rescued cortical and trabecular BMD (bone only without bone marrow) in Klotho$^{-/-}$/VDR$^{\Delta/\Delta}$ but not in Fgf23$^{-/-}$/VDR$^{\Delta/\Delta}$ compound mutants (Fig. 1A and Supplemental Fig. S1A). To analyze bone mineralization at the material level in more detail, we performed qBEI analyses of the bone mineralization density distribution in the femoral midshaft. In agreement with the μCT data, the reduced weighted mean calcium content (CaMean) and increased extent of hypomineralized bone areas (CaLow) observed in Klotho$^{-/-}$ and Fgf23$^{-/-}$ mutants were completely normalized in Klotho$^{-/-}$/VDR$^{\Delta/\Delta}$ compound mutants (Fig. 1B). However, CaLow remained increased in Fgf23$^{-/-}$/VDR$^{\Delta/\Delta}$ compound mutants, relative to VDR$^{\Delta/\Delta}$ mice

(Fig. 1B). Both μCT imaging and qBEI do not detect osteoid. To quantify osteoid volume and thickness, we performed histomorphometric analyses of longitudinal femur sections. As shown in Fig. 1C and Supplemental Fig. S1B, osteoid volume and thickness were profoundly increased in femoral cortical and cancellous bone of Klotho$^{-/-}$ and Fgf23$^{-/-}$ mutants, relative to wild-type and VDR$^{\Delta/\Delta}$ controls, indicating severe osteomalacia in Klotho- and Fgf23-deficient mice. Osteoid volume and thickness returned to VDR$^{\Delta/\Delta}$ control levels in Klotho$^{-/-}$/VDR$^{\Delta/\Delta}$ mice, but remained slightly, but significantly elevated in Fgf23$^{-/-}$/VDR$^{\Delta/\Delta}$ compared with VDR$^{\Delta/\Delta}$ mice (Fig. 1C and Supplemental Fig. 1B). Taken together, these results suggest that the mineralization defect observed in Klotho$^{-/-}$ mice is entirely owing to augmented vitamin D signaling. In contrast, ablation of vitamin D signaling in Fgf23$^{-/-}$/VDR$^{\Delta/\Delta}$ mice largely, but not completely, rescued the mineralization defect, indicating that Fgf23 per se may have a Klotho-independent role in bone mineralization.

Ablation of VDR signaling normalizes expression of PPi-regulating genes and of OPN in Klotho$^{-/-}$/VDR$^{\Delta/\Delta}$ but not in Fgf23$^{-/-}$/VDR$^{\Delta/\Delta}$ mice.

Next, we sought to elucidate the molecular mechanisms underlying the impairment in bone mineralization in Klotho- and Fgf23-deficient mice. Because 1,25(OH)$_2$D$_3$ has been shown to regulate genes involved in PPi metabolism,[14] we analyzed femoral mRNA expression of genes involved in PPi production, transportation, and hydrolysis, in addition to another well-known and 1,25(OH)$_2$D$_3$-induced mineralization inhibitor, OPN. PPi is produced intracellularly by ectonucleotide pyrophosphatase/phosphodiesterase 1 and 3 (ENPP1 and ENPP3).[33] The transmembrane protein ANK then mediates the extracellular transport of PPi.[34] PPi in the extracellular matrix is hydrolyzed to Pi by the ecto-enzyme tissue nonspecific alkaline phosphatase (TNAP).[35]

Relative to WT mice, femurs from VDR$^{\Delta/\Delta}$ mice showed increased mRNA expression of ENPP3 and TNAP. The mRNA abundance of ANK, ENPP1, and OPN was significantly increased in femurs of Klotho$^{-/-}$ and Fgf23$^{-/-}$ mice compared with WT and VDR$^{\Delta/\Delta}$ mice (Fig. 2A). In contrast, mRNA expression of TNAP was suppressed in Klotho$^{-/-}$ mice compared with WT and VDR$^{\Delta/\Delta}$ mice (Fig. 2A). TNAP mRNA abundance was increased either by loss of vitamin D signaling in VDR$^{\Delta/\Delta}$, Klotho$^{-/-}$/VDR$^{\Delta/\Delta}$, and Fgf23$^{-/-}$/VDR$^{\Delta/\Delta}$ mice or lack of Fgf23 signaling in Fgf23$^{-/-}$ and Fgf23$^{-/-}$/VDR$^{\Delta/\Delta}$
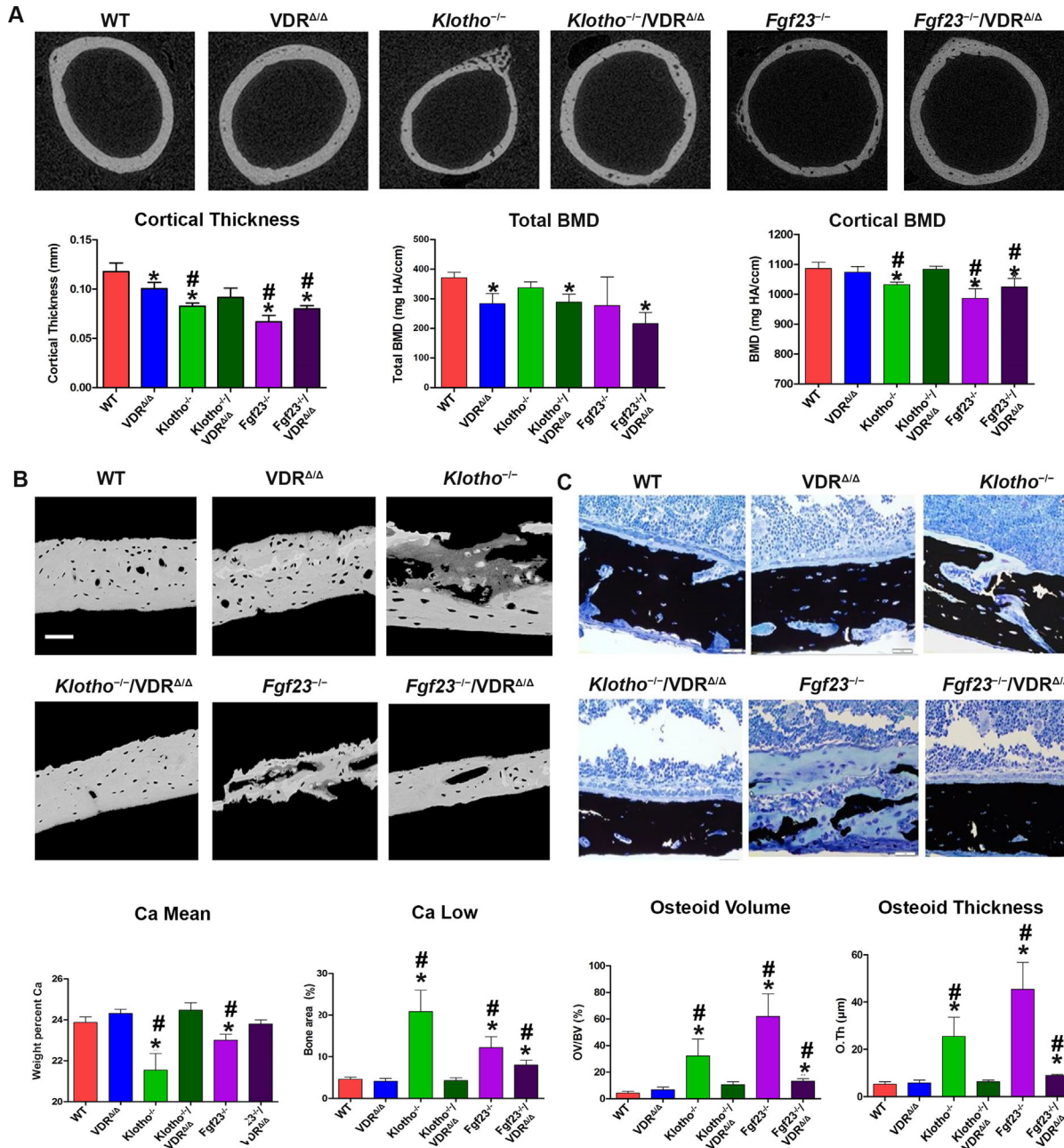
Fig. 1. VDR ablation normalizes bone mineralization defect in $Klotho^{-/-}$/VDR$^{\Delta/\Delta}$ but not in $Fgf23^{-/-}$/VDR$^{\Delta/\Delta}$ compound mutant mice. (*A*) Representative μCT images (upper panels), as well as cortical thickness, total BMD, and cortical BMD analyzed by μCT in the femoral midshaft region, (*B*) representative qBEI images (×200, upper panels), as well as Ca Mean and Ca Low measured by qBEI in femoral cortical bone, and (*C*) von Kossa/McNeal staining of undecalcified plastic sections of distal femurs (upper panels) and histomorphometric analyses of osteoid volume and osteoid thickness in femoral cortical bone of 4-week-old WT, VDR$^{\Delta/\Delta}$, $Klotho^{-/-}$, $Fgf23^{-/-}$, $Klotho^{-/-}$/VDR$^{\Delta/\Delta}$, and $Fgf23^{-/-}$/VDR$^{\Delta/\Delta}$ mice. Each data point is the mean ± SEM of at least 5 animals per genotype. Scale bar = 50 μm (*C*). *$p < 0.05$ versus WT; #$p < 0.05$ versus VDR$^{\Delta/\Delta}$ mice.

mice, suggesting an inhibitory role of vitamin D and Fgf23 on bony *TNAP* expression. The expression of *PHEX* was unchanged in $Klotho^{-/-}$ and $Klotho^{-/-}$/VDR$^{\Delta/\Delta}$ mutants but profoundly upregulated in mice lacking Fgf23 (Fig. 2*A*).

Ablation of VDR signaling in $Klotho^{-/-}$/VDR$^{\Delta/\Delta}$ mice normalized the mRNA abundance of *ENPP1, ANK, OPN,* and *TNAP* relative to VDR$^{\Delta/\Delta}$ control levels. However, lack of vitamin D signaling in

$Fgf23^{-/-}$/VDR$^{\Delta/\Delta}$ mice failed to normalize the mRNA expression of *ANK, ENPP1, ENPP3, OPN, TNAP,* and *PHEX,* which all remained elevated relative to VDR$^{\Delta/\Delta}$ mice (Fig. 2*A*). Based on the increased expression of *ANK, ENPP1,* and *OPN* in femurs of $Klotho^{-/-}$ and $Fgf23^{-/-}$ mice, we hypothesized that the impaired bone mineralization in $Klotho^{-/-}$ and $Fgf23^{-/-}$ mice may be because of accumulation of PPi and OPN in the extracellular matrix. To test

this hypothesis, we quantified the amount of PPi and OPN in extracts of femurs by a biochemical assay and Western blotting, respectively. The PPi concentration per mg wet weight was about fivefold and 10-fold higher in femurs from $Klotho^{-/-}$ (15.40 ± 6.70 μmol/mg) and $Fgf23^{-/-}$ (16.38 ± 2.83 μmol/mg) mice, relative to WT (2.95 ± 2.49 μmol/mg) and $VDR^{\Delta/\Delta}$ (1.64 ± 0.94 μmol/mg) mice, respectively (Fig. 2B). In addition, OPN protein expression was about twofold higher in femurs from $Klotho^{-/-}$ and $Fgf23^{-/-}$ mice relative to WT controls (Fig. 2C). In line with the notion that OPN is positively regulated by 1,25(OH)$_2$D$_3$, OPN expression was lower in $VDR^{\Delta/\Delta}$ compared with WT mice (Fig. 2C). Much to our surprise, the femoral PPi concentration was completely normalized in both $Klotho^{-/-}$/$VDR^{\Delta/\Delta}$ (2.65 ± 1.29 μmol/mg) and $Fgf23^{-/-}$/$VDR^{\Delta/\Delta}$ (3.15 ± 1.58 μmol/mg) compound mutants (Fig. 2B). However, osteopontin protein expression returned to $VDR^{\Delta/\Delta}$ control levels only in $Klotho^{-/-}$/$VDR^{\Delta/\Delta}$ but not in $Fgf23^{-/-}$/$VDR^{\Delta/\Delta}$ mice (Fig. 2C). In analogy to the Western blot findings, immunohistochemistry confirmed the profoundly increased expression of OPN in cortical and cancellous bone of $Klotho^{-/-}$, $Fgf23^{-/-}$, and $Fgf23^{-/-}$/$VDR^{\Delta/\Delta}$ mice (Fig. 2D and Supplemental Fig. 1C). Collectively, these results suggest that the mineralization defect found in $Klotho^{-/-}$ and $Fgf23^{-/-}$ mice is mainly caused by 1,25(OH)$_2$D$_3$-driven accumulation of PPi and OPN in the extracellular matrix. In addition, lack of Fgf23 signaling per se appears to upregulate OPN protein expression because OPN expression remained elevated in $Fgf23^{-/-}$/$VDR^{\Delta/\Delta}$ mice in the absence of vitamin D signaling.

1,25(OH)$_2$D$_3$ increases mRNA expression of ENPP1, ENPP3, and OPN, whereas FGF23 suppresses mRNA expression of TNAP in differentiated osteoblasts

To further examine the mechanisms underlying the effects of 1,25(OH)$_2$D$_3$ and Fgf23 on bone mineralization, we isolated osteoblasts from newborn WT mice and treated them with 1,25(OH)$_2$D$_3$ and recombinant FGF23 (rFGF23) in vitro. In agreement with the reported data from Lieben and colleagues,[14] we found that 1,25(OH)$_2$D$_3$ stimulated the mRNA expression of ENPP1, ENPP3, and OPN in a VDR-dependent manner but not that of ANK or TNAP (Fig. 3A). Treatment of differentiated WT osteoblasts with 10 or 100 ng/mL rFGF23 for 24 hours did not alter expression of ENPP1, ENPP3, OPN, or ANK but dose-dependently suppressed TNAP expression (Fig. 3B). To analyze whether the suppression of TNAP by FGF23 requires the presence of Klotho, we isolated osteoblasts from newborn $Klotho^{-/-}$ mice and treated them with rFGF23. Similar to WT osteoblasts, rFGF23 dose-dependently suppressed TNAP mRNA expression in differentiated osteoblasts from $Klotho^{-/-}$ mice, showing that this effect is Klotho independent (Fig. 3B). To show that rFGF23 regulates TNAP not only at the transcriptional but also at the protein level, we treated differentiated osteoblasts with rFGF23 for 48 hours and subsequently assessed ALP expression using NBT/BCIP staining. As shown in Fig. 3C, rFGF23 suppressed ALP activity in vitro in differentiated osteoblasts isolated from WT and $Klotho^{-/-}$ mice, indicating that rFGF23 is a Klotho-independent regulator of TNAP also at the protein level. In addition, ALP activity was increased in differentiated osteoblasts isolated from $Fgf23^{-/-}$ but not those isolated from $Klotho^{-/-}$ mice (Fig. 3C), showing that lack of Fgf23 signaling leads to a Klotho-independent, cell-autonomous increase in ALP activity.

Fgf23 regulates TNAP through the FGFR3-ERK pathway

To determine the signaling pathway through which Fgf23 suppresses TNAP in osteoblasts, we treated differentiated

osteoblasts isolated from WT mice with rFGF23, alone or in combination with FGF receptor inhibitors. As shown in Fig. 4, the FGF23-induced suppression of TNAP expression was blocked in the presence of pan-FGFR (Fig. 4A), FGFR3 (Fig. 4C), and ERK1/2 inhibitors (Fig. 4D) but not in the presence of an FGFR1 inhibitor (Fig. 4B). To additionally assess TNAP enzyme activity in this experiment, we measured phosphate concentrations in the cell culture medium. It is known that TNAP can produce inorganic phosphate by cleavage of β-glycerophosphate,[36] which is a component of the osteoblast differentiation medium. In agreement with the data on mRNA expression of TNAP, the inorganic phosphate concentration in the cell culture medium was reduced by rFGF23 only in cells cotreated with the FGFR1 inhibitor (Fig. 4B) but not when osteoblasts were cotreated with rFGF23 and pan-FGFR, ERK1/2, or FGFR3 inhibitors (Fig. 4A–C). Collectively, our data suggest that FGF23 regulates TNAP and thereby phosphate production through the FGFR3-ERK pathway.

Finally, to compare the sensitivity of the FGFR3-mediated suppression of TNAP expression in osteoblasts with a known canonical FGFR1/Klotho-mediated signaling mechanism, we performed in vitro dose-response experiments in osteoblasts and in isolated segments of distal renal tubules.[5] We found that ~100-fold higher concentrations of FGF23 were needed to significantly suppress TNAP in osteoblasts (≥10 ng/mL), relative to induction of the sodium-chloride cotransporter NCC in renal distal tubules (≥0.1 ng/mL), indicating that FGFR3-mediated signaling requires much higher concentrations of the ligand FGF23 than the canonical FGFR1/Klotho signaling mechanism (Fig. 4E).

FGF23 regulates OPN indirectly through TNAP

So far, our data suggest that FGF23 is a transcriptional regulator of TNAP, whereas OPN does not seem to be regulated by FGF23 at the transcriptional level. Because inorganic phosphate is a well-known stimulator of OPN secretion,[37–40] we hypothesized that FGF23 may suppress OPN secretion indirectly through changes in the extracellular inorganic phosphate concentration caused by altered TNAP enzyme activity. To test this hypothesis, we treated WT osteoblasts for 48 hours with rFGF23 or a neutralizing anti-FGF23 antibody in the absence and presence of levamisole, a standard inhibitor of TNAP enzyme activity.[36] As shown in Fig. 5A and B, rFGF23 suppressed, whereas the anti-FGF23 antibody increased, OPN protein expression. In line with our hypothesis, the anti-FGF23 antibody-induced upregulation of OPN protein expression could be blocked by levamisole (Fig. 5C), suggesting that rFGF23 regulates OPN indirectly through TNAP. Interestingly, inhibition of TNAP activity by levamisole increased OPN mRNA and protein expression in WT osteoblasts (Fig. 5C, also shown in Fig. 5E). We hypothesize that this effect is the result of accumulation of PPi in the culture medium because of inhibition of its major degrading enzyme TNAP. Similar to phosphate, PPi is known to stimulate OPN secretion.[41,42] As shown in Fig. 5C, levamisole treatment increased PPi concentration in the culture medium with or without anti-FGF23 antibody. Conversely, treatment with anti-FGF23 antibody decreased PPi levels compared with vehicle (Fig. 5C), probably because of the increased TNAP activity as a consequence of loss of FGF23 signaling (vide infra in Fig. 5E).

Next, we isolated osteoblasts from newborn WT, $VDR^{\Delta/\Delta}$, $Klotho^{-/-}$, $Fgf23^{-/-}$, $Fgf23^{-/-}$/$VDR^{\Delta/\Delta}$, and $Klotho^{-/-}$/$VDR^{\Delta/\Delta}$ compound
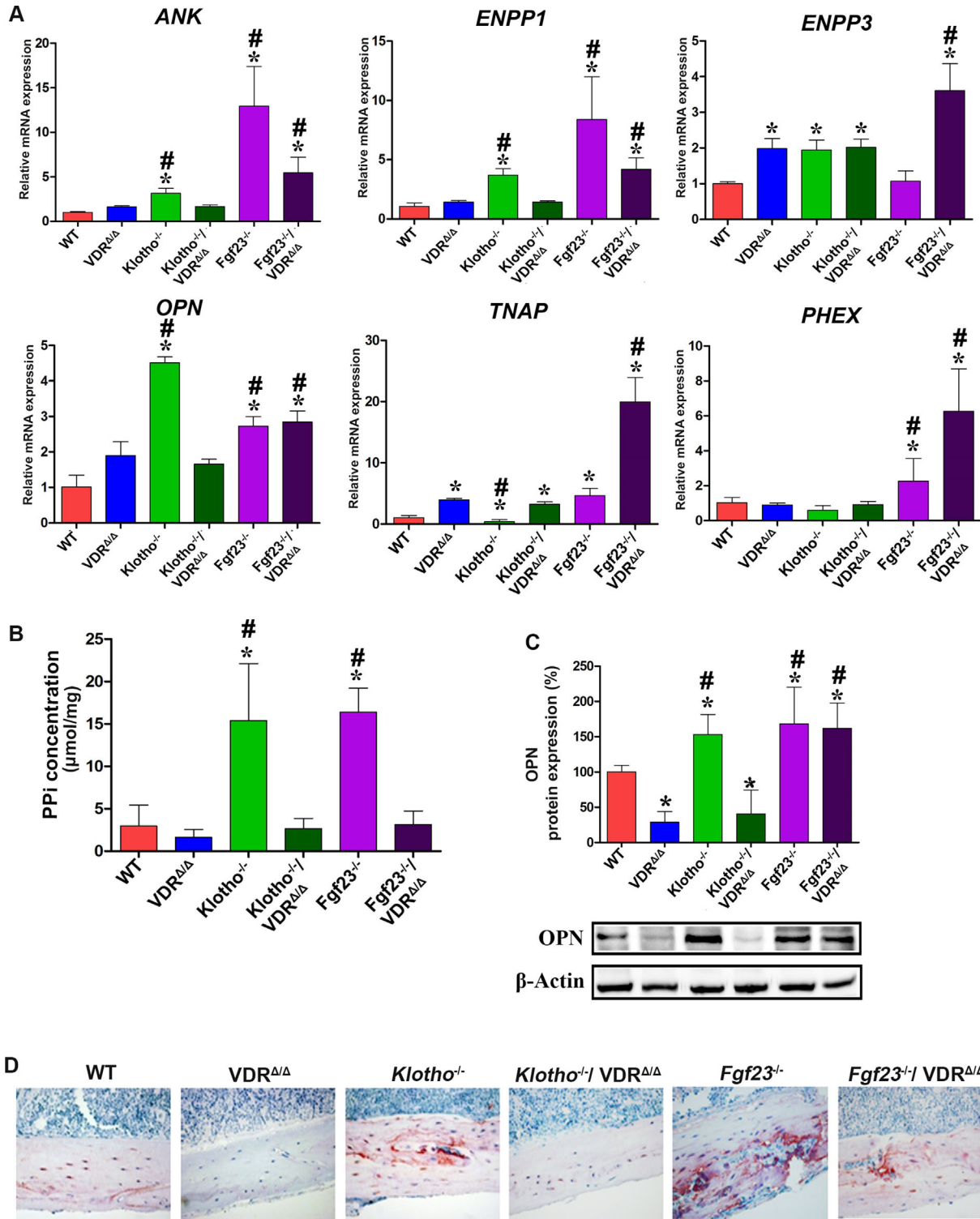
Fig. 2. Expression of PPi-regulating genes and OPN is normalized in *Klotho*$^{−/−}$/VDR but not in *Fgf23*$^{−/−}$/VDR mice. (*A*) *ANK, ENPP1, ENPP3, OPN, TNAP,* and *PHEX* mRNA abundance assessed by qRT-PCR in total RNA isolated from whole femurs, (*B*) PPi levels in extracts of whole femurs, (*C*) quantification of OPN protein expression by Western blotting in total protein preparations of whole femurs, and (*D*) immunohistochemical staining of osteopontin protein expression in femoral cortical bone in 4-week-old WT, VDR$^{Δ/Δ}$, *Klotho*$^{−/−}$, *Fgf23*$^{−/−}$, *Klotho*$^{−/−}$/VDR$^{Δ/Δ}$, and *Fgf23*$^{−/−}$/VDR$^{Δ/Δ}$ mice. Each data point is the mean ± SEM of at least 5 animals per genotype. *$p < 0.05$ versus WT; #$p < 0.05$ versus VDR$^{Δ/Δ}$ mice.
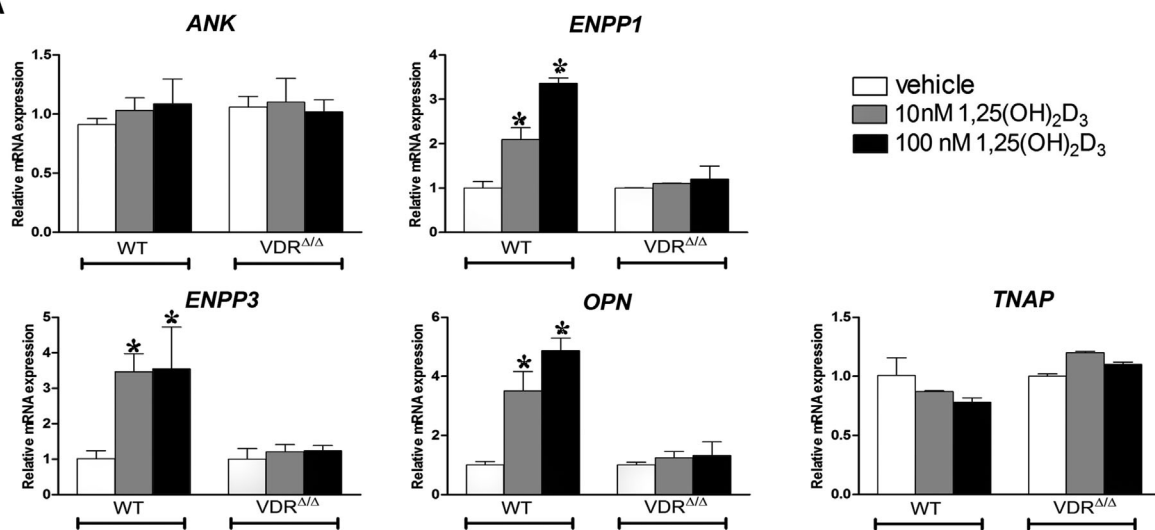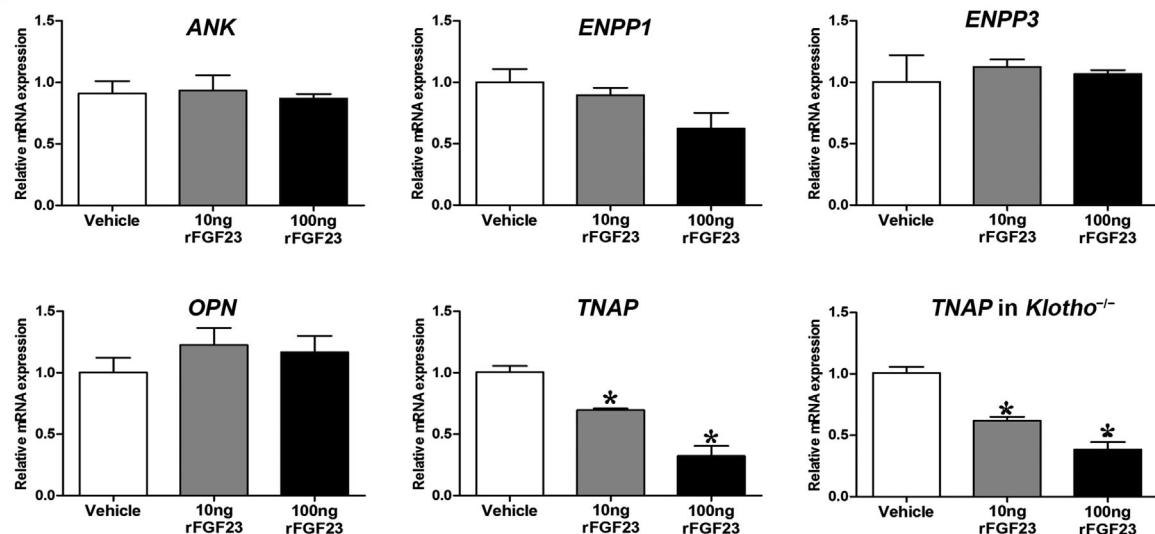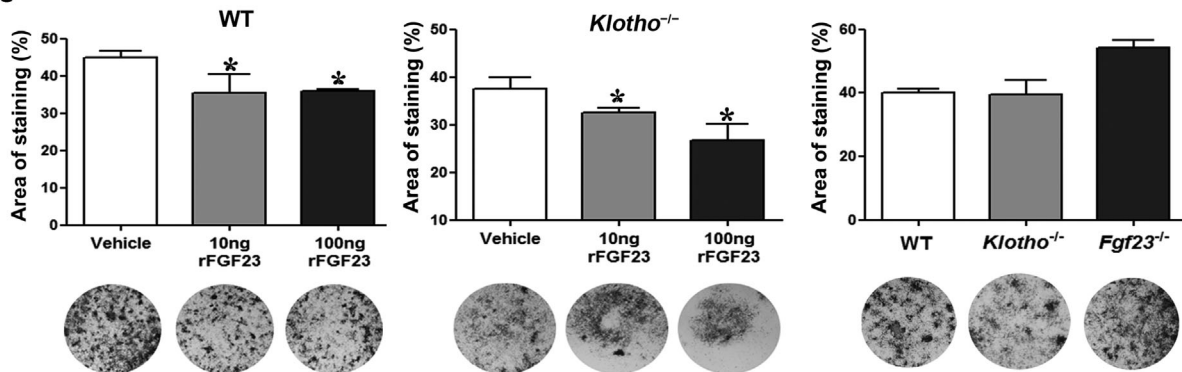
Fig. 3. $1,25(OH)_2D_3$ but not FGF23 regulates *ENPP1, ENPP3,* and *OPN* in differentiated osteoblasts in vitro. (*A*) mRNA abundance of *ANK, ENPP1, ENPP3, OPN,* and *TNAP* in differentiated calvarial osteoblasts isolated from newborn WT and VDR$^{\Delta/\Delta}$ mice treated for 24 hours with 10^{-7}-10^{-8} M $1,25(OH)_2D_3$ or vehicle. (*B*) mRNA abundance of *ANK, ENPP1, ENPP3, OPN,* and *TNAP* in differentiated calvarial osteoblasts isolated from newborn WT or *Klotho*$^{-/-}$ mice after a 24-hour treatment with rFGF23 or vehicle. (*C*) Percent NBT/BCIP-stained area in cultures of differentiated calvarial osteoblasts isolated from newborn WT, *Klotho*$^{-/-}$, and *Fgf23*$^{-/-}$ mice; (left and middle panels) after treatment with vehicle or rFGF23 for 24 hours, (right panel) untreated osteoblasts from *Klotho*$^{-/-}$ and *Fgf23*$^{-/-}$ mice. Each data point is the mean $\pm$ SEM of 4 experimental samples. $^*p < 0.05$ versus vehicle or WT.
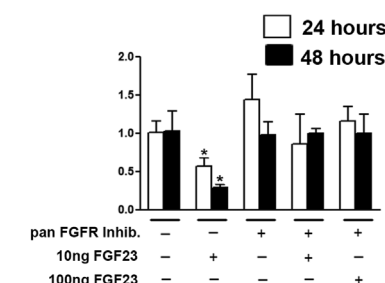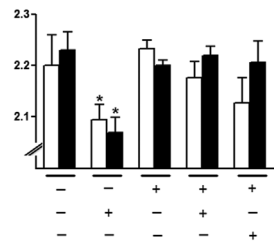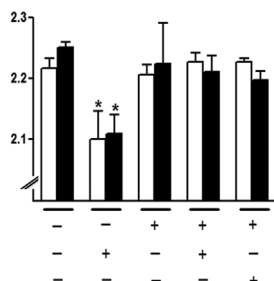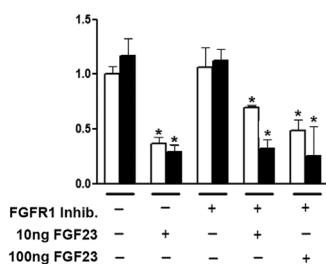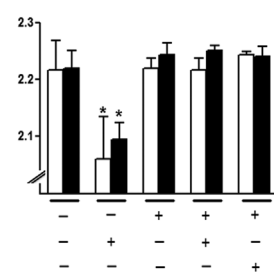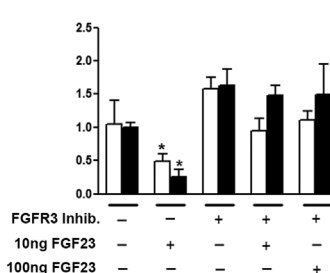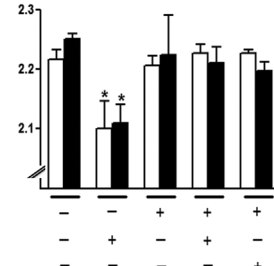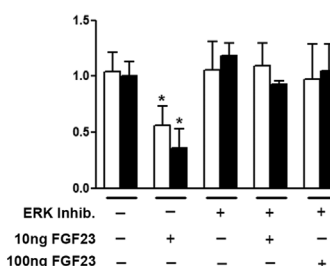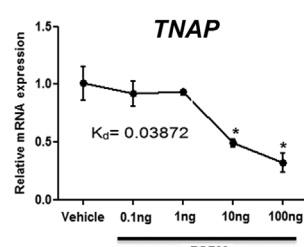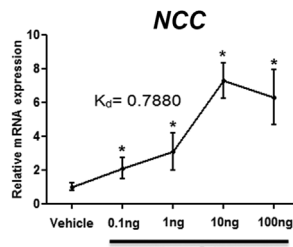
Fig. 4. FGF23 regulates *TNAP* through the FGFR3-ERK pathway. (*A–D*) mRNA abundance of *TNAP* and inorganic phosphate concentration in cell culture supernatant of differentiated calvarial osteoblasts isolated from WT animals after treatment with rFGF23 alone or in combination with a pan FGFR inhibitor (*A*), FGFR1 inhibitor (*B*), FGFR3 inhibitor (*C*), or ERK1/2 inhibitor (*D*). (*E*) Dose-response curves for sodium-chloride cotransporter (NCC) mRNA expression in isolated segments of distal renal tubules and of TNAP mRNA expression in differentiated calvarial osteoblasts, 24 hours after treatment with different doses of rFGF23. Each data point is the mean ± SEM of 4 experimental samples in *A–D* and 3 to 6 samples per dose in *E*. *$p < 0.05$ versus vehicle.
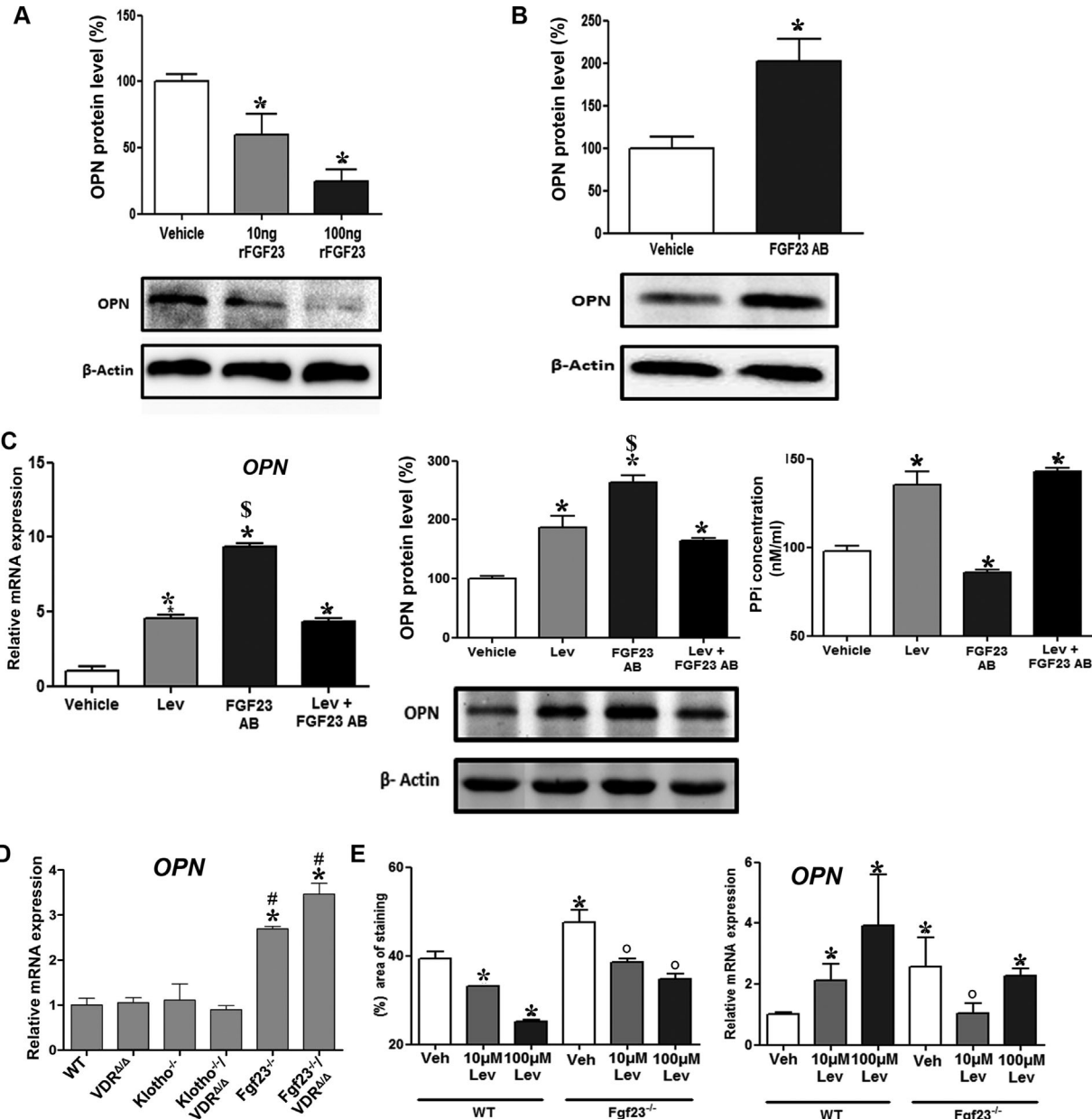
Fig. 5. FGF23 regulates OPN expression through TNAP. (*A, B*) OPN protein level in differentiated WT calvarial osteoblasts, 48 hours after treatment with rFGF23 (*A*) or anti-FGF23 antibody (FGF23 AB) (*B*). (*C*) *OPN* mRNA, OPN protein expression, and PPi concentration in cultures of WT differentiated calvarial osteoblasts after treatment with levamisole alone or in combination with FGF23 AB for 48 hours. (*D*) *OPN* mRNA abundance in differentiated calvarial osteoblasts isolated from newborn WT, VDR$^{\Delta/\Delta}$, *Klotho*$^{-/-}$, *Fgf23*$^{-/-}$, *Klotho*$^{-/-}$/VDR$^{\Delta/\Delta}$, and *Fgf23*$^{-/-}$/VDR$^{\Delta/\Delta}$ mice. (*E*) Percent NBT/BCIP-stained area and *OPN* mRNA expression in cultures of differentiated calvarial osteoblasts isolated from newborn WT and *Fgf23*$^{-/-}$ mice after 48 hours of treatment with vehicle or levamisole (Lev). Each data point is the mean ± SEM of 4 experimental samples. $^*p < 0.05$ versus vehicle or vehicle-treated WT cells; $^\$p < 0.05$ versus levamisole (Lev) treatment; $^\#p < 0.05$ versus VDR$^{\Delta/\Delta}$; $^\circ p < 0.05$ versus vehicle-treated *Fgf23*$^{-/-}$ cells.

mutants and examined OPN mRNA expression. Differentiated primary osteoblasts isolated from *Fgf23*$^{-/-}$ and *Fgf23*$^{-/-}$/VDR$^{\Delta/\Delta}$ mice, but not those isolated from *Klotho*$^{-/-}$ mice, showed increases in OPN mRNA expression compared with cells isolated from WT animals (Fig. 5*D*). As expected, addition of levamisole suppressed alkaline phosphatase staining in osteoblast cultures from WT and *Fgf23*$^{-/-}$ mice (Fig. 5*E*). An amount of 10 μM levamisole suppressed

ALP staining in osteoblasts from *Fgf23*$^{-/-}$ mice to levels similar to those observed in WT vehicle controls, and completely corrected the increased OPN mRNA expression in osteoblasts from *Fgf23*$^{-/-}$ mice (Fig. 5*E*). Taken together, our data provide strong evidence that the regulation of OPN protein and mRNA expression by FGF23 is a cell-autonomous, but indirect, effect mediated through the regulation of TNAP expression.

Discussion

It has long been an enigma why bone mineralization is impaired in $Fgf23^{-/-}$ and $Klotho^{-/-}$ mice despite the presence of hypercalcemia and hyperphosphatemia. Here, we show for the first time to our knowledge that the osteomalacia in $Fgf23^{-/-}$ and $Klotho^{-/-}$ mice is caused by accumulation of PPi and OPN in bone tissue. In $Klotho^{-/-}$ mice, the mineralization defect is solely driven by 1,25(OH)$_2$D$_3$-induced upregulation of PPi-producing enzymes, of the PPi transporter ANK, and of OPN. In $Fgf23^{-/-}$ mice, the mineralization defect has two components, a 1,25(OH)$_2$D$_3$-driven component similar to $Klotho^{-/-}$ mice, and a component driven by lack of Fgf23, leading to additional accumulation of OPN. In the current study, we identified Fgf23 as a strong transcriptional suppressor of TNAP in osteoblastic cells, acting through FGFR3 in a Klotho-independent manner. In agreement with our findings, it was previously reported that Fgf23 binds to FGFR3 in vitro in chondrocytes.[43] Hence, we hypothesize that Fgf23 secreted from osteocytes forms an autocrine/paracrine feedback loop in bone to indirectly regulate OPN secretion through TNAP. This novel paradigm is shown in Fig. 6.

Our findings are in line with a previous report showing that the mineralization defect in $Fgf23^{-/-}$ mice was partially rescued by genetic ablation of OPN.[7] The current study provides an explanation for the only partial rescue of bone mineralization in $Fgf23^{-/-}/OPN^{-/-}$ compound mutants because PPi was probably still elevated in these mice because of increased serum 1,25(OH)$_2$D$_3$. Moreover, additional ablation of PTH in $Klotho^{-/-}$ mice was reported to reduce OPN levels and to largely rescue the skeletal abnormalities, despite elevated serum levels of 1,25(OH)$_2$D$_3$.[12] In contrast, $Klotho^{-/-}/VDR^{\Delta/\Delta}$ compound mutants showed normal bone mineralization in the presence of moderately elevated PTH serum levels in the present study (Table 1). We don't have a good explanation for this discrepancy. However, it is conceivable that PTH and 1,25(OH)$_2$D$_3$ interact in osteocytes in the regulation of molecules involved in mineralization.

The present study has shown that the mineralization defect observed in $Klotho^{-/-}$ mice and partially that in $Fgf23^{-/-}$ mice is caused by higher-circulating 1,25(OH)$_2$D$_3$ and subsequent increases in bony PPi and OPN concentrations. Our in vivo and in vitro data support the study by Lieben and colleagues,[14] showing that 1,25(OH)$_2$D$_3$ inhibits bone mineralization locally in osteoblasts and osteocytes by stimulating the transcription of $ENPP1$ and 3, ANK, and OPN. Although we were unable to confirm the previously reported 1,25(OH)$_2$D$_3$-induced stimulation of ANK expression[14] in our experiments, our study and the study by Lieben and colleagues[14] provide strong evidence that 1,25(OH)$_2$D$_3$ is an important regulator of inhibitors of bone mineralization such as PPi and OPN.

In contrast to our data, it was previously reported that osteoblasts isolated from Klotho KO display a cell-autonomous defect in bone mineralization.[12] However, several independent lines of evidence in our experiments suggest that Klotho lacks a role in bone mineralization. 1) Despite loss of Klotho, $Klotho^{-/-}/VDR^{\Delta/\Delta}$ compound mutant displayed normal bone mineralization and were indistinguishable from $VDR^{\Delta/\Delta}$ controls in terms of mRNA abundance of $ENPP1$, ANK, OPN, and $TNAP$, as well as in terms of PPi concentrations and OPN protein expression in bone. 2) Osteoblasts isolated from $Klotho^{-/-}$ mice showed normal mineralization in culture. 3) FGF23 suppressed TNAP transcription in osteoblasts through an FGFR3-mediated, Klotho-independent signaling mechanism. Taken together, the

evidence garnered from these distinct experimental approaches support the notion that Klotho lacks a 1,25(OH)$_2$D$_3$-independent role in bone mineralization.

Despite profound increases in the mRNA abundance of genes involved in PPi production and transportation, bone PPi levels were normal in $Fgf23^{-/-}/VDR^{\Delta/\Delta}$ mice. We hypothesize that the 20-fold higher mRNA expression of $TNAP$ in $Fgf23^{-/-}/VDR^{\Delta/\Delta}$ compound mutants, relative to WT mice, counteracted the increased PPi production and transportation. It is known that PPi present in the ECM is hydrolyzed by $TNAP$ to form Pi, which, in turn, contributes to the mineralization process. The upregulation of $TNAP$ in $Fgf23^{-/-}/VDR^{\Delta/\Delta}$ mice can be explained by the lacking suppressive effect of Fgf23 on $TNAP$ transcription in these mice. Based on our in vitro data, we further hypothesize that the increased enzymatic activity of TNAP in $Fgf23^{-/-}/VDR^{\Delta/\Delta}$ mice results in increased extracellular phosphate concentrations, which, in turn, upregulate the secretion of the mineralization inhibitor OPN. A limitation of the current study is that we do not provide direct evidence that phosphate concentrations are indeed elevated in osteocyte lacunae in $Fgf23^{-/-}/VDR^{\Delta/\Delta}$ mice in vivo. However, this is currently technically not feasible.

The human genetic disease hypophosphatasia is caused by loss-of-function mutations in $TNAP$, leading to hypomineralized bones, spontaneous fractures, and elevated extracellular concentration of PPi.[44] Similarly, osteoblasts isolated from $TNAP^{-/-}$ mice are unable to initiate mineralization in vitro.[45] Conversely, TNAP overexpression leads to increased skeletal mineralization.[46] In $Fgf23^{-/-}/VDR^{\Delta/\Delta}$ mice, bone mineralization remained impaired in the presence of 20-fold increased TNAP expression in our study. The explanation for this apparent discrepancy is 1) that increased TNAP expression in $Fgf23^{-/-}/VDR^{\Delta/\Delta}$ mice was able to normalize, but not to lower, PPi concentration in bone because of augmented PPi production and transportation at the same time in these mice, and 2) that the mineralization inhibitor OPN remained elevated. An open question in this context is why increased mRNA expression of PHEX found in $Fgf23^{-/-}$ and $Fgf23^{-/-}/VDR^{\Delta/\Delta}$ mice in our study was not able to normalize OPN protein expression in bone. The neutral endopeptidase PHEX cleaves excess amounts of OPN and SIBLING protein-derived ASARM peptides during the mineralization process.[47] The importance of PHEX is illustrated by the fact that loss-of-function mutations in PHEX lead to severe impairment of bone mineralization because of accumulation of ASARM peptides and OPN in the matrix[47] and because of subsequent excessive osteocytic secretion of Fgf23.[48]

In the current study, we focused on the mechanisms involved in the mineralization defect found in $Klotho^{-/-}$ and $Fgf23^{-/-}$ mice. However, not only loss of Fgf23 function but also gain of FGF23 function causes impaired bone mineralization, leading to osteomalacia or rickets. It is currently thought that excessive FGF23 impairs bone mineralization through its phosphaturic effects and subsequent hypophosphatemia. However, based on the findings reported here, it might be possible that elevated FGF23 secretion may suppress TNAP locally in osteocytes and osteoblasts, which, in turn, may lead to accumulation of PPi. It is currently unknown whether such a mechanism may contribute to the defect in bone mineralization induced by excessive FGF23 secretion.

Our study has uncovered a novel physiological role of FGF23 in osteocytes as a regulator of TNAP expression and OPN secretion. The presumably high extracellular concentration of the locally produced FGF23 in the osteocyte canalicular system may compensate for the relatively low binding affinity of the
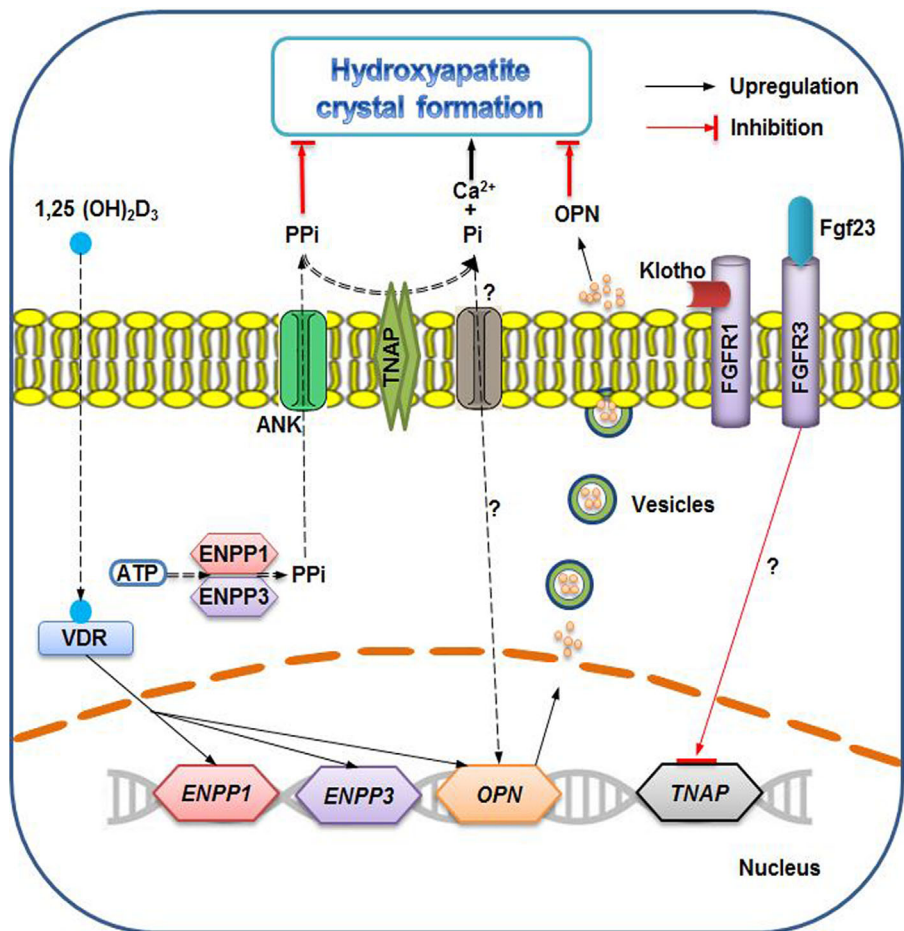
Fig. 6. Proposed model of FGF23-FGFR3 signaling and its local role for mineralization in osteoblasts and osteocytes. The vitamin D hormone inhibits mineralization by stimulating the intracellular production of pyrophosphate (PPi) through increased transcription of ENPP1 and 3, as well as by augmenting the expression of the mineralization inhibitor OPN. FGF23 binds to the FGFR3 receptor in a Klotho-independent fashion, leading to transcriptional suppression of TNAP via ERK1/2 activation. Decreased TNAP activity at the plasma membrane in turn leads to decreased degradation of pyrophosphate and lower inorganic phosphate production, both effects causing impaired bone mineralization. Extracellular phosphate stimulates OPN transcription and secretion by an unknown signaling mechanism. Therefore, FGF23 signaling indirectly downregulates OPN secretion via suppressing TNAP expression. In this model, the extracellular concentration of FGF23 locally regulates mineralization in osteoblasts and osteocytes in an autocrine or paracrine fashion by controlling TNAP, a central molecule in the mineralization process.

FGFR3-mediated suppression of *TNAP* transcription by FGF23 reported here. Hence, this Klotho-independent signaling pathway may be important for the fine-tuning of mineralization around osteocytes and osteoblasts.

Disclosures

All authors state that they have no conflicts of interest.

Acknowledgments

Authors' roles: Study design: SKM, OA, and RGE. Study conduct and data collection: SKM, PR, and UZ. Data analysis: SKM, PR, and OA. Data interpretation: SKM, PR, KK, OA, and RGE. Drafting manuscript: SKM, PR, OA, and RGE. All authors revised the manuscript content and approved the final version of the manuscript. SKM takes responsibility for the integrity of the data analysis.

References

1. Saito H, Maeda A, Ohtomo S, et al. Circulating FGF-23 is regulated by 1alpha,25-dihydroxyvitamin D3 and phosphorus in vivo. J Biol Chem. 2005;280(4):2543–9.

2. Andrukhova O, Zeitz U, Goetz R, Mohammadi M, Lanske B, Erben RG. FGF23 acts directly on renal proximal tubules to induce phosphaturia through activation of the ERK1/2-SGK1 signaling pathway. Bone. 2012;51(3):621–8.

3. Shimada T, Hasegawa H, Yamazaki Y, et al. FGF-23 is a potent regulator of vitamin D metabolism and phosphate homeostasis. J Bone Miner Res. 2004;19(3):429–35.

4. Andrukhova O, Smorodchenko A, Egerbacher M, et al. FGF23 promotes renal calcium reabsorption through the TRPV5 channel. EMBO.J. 2014;33(3):229–46.

5. Andrukhova O, Slavic S, Smorodchenko A, et al. FGF23 regulates renal sodium handling and blood pressure. EMBO Mol Med. 2014;6(6):744–59.

6. Kuro-o M, Matsumura Y, Aizawa H, et al. Mutation of the mouse klotho gene leads to a syndrome resembling ageing. Nature. 1997;390(6655):45–51.

7. Yuan Q, Jiang Y, Zhao X, et al. Increased osteopontin contributes to inhibition of bone mineralization in FGF23-deficient mice. J Bone Miner Res. 2014;29(3):693–704.

8. Urakawa I, Yamazaki Y, Shimada T, et al. Klotho converts canonical FGF receptor into a specific receptor for FGF23. Nature. 2006; 444(7120):770–4.

9. Anour R, Andrukhova O, Ritter E, Zeitz U, Erben RG. Klotho lacks a vitamin D independent physiological role in glucose homeostasis, bone turnover, and steady-state PTH secretion in vivo. PLoS One. 2012;7(2):e31376.

10. Sitara D, Razzaque MS, Hesse M, et al. Homozygous ablation of fibroblast growth factor-23 results in hyperphosphatemia and impaired skeletogenesis, and reverses hypophosphatemia in Phex-deficient mice. Matrix Biol. 2004;23(7):421–32.

11. Hesse M, Frohlich LF, Zeitz U, Lanske B, Erben RG. Ablation of vitamin D signaling rescues bone, mineral, and glucose homeostasis in Fgf-23 deficient mice. Matrix Biol. 2007;26(2):75–84.

12. Yuan Q, Sato T, Densmore M, et al. Deletion of PTH rescues skeletal abnormalities and high osteopontin levels in Klotho-/- mice. PLoS Genet. 2012;8(5):e1002726.

13. Sapir-Koren R, Livshits G. Bone mineralization and regulation of phosphate homeostasis. IBMS BoneKEy. 2011;8(6):286–300.

14. Lieben L, Masuyama R, Torrekens S, et al. Normocalcemia is maintained in mice under conditions of calcium malabsorption by vitamin D-induced inhibition of bone mineralization. J Clin Invest. 2012;122(5):1803–15.

15. Russell RG, Bisaz S, Donath A, Morgan DB, Fleisch H. Inorganic pyrophosphate in plasma in normal persons and in patients with hypophosphatasia, osteogenesis imperfecta, and other disorders of bone. J Clin Invest. 1971;50(5):961–9.

16. Gurley KA, Chen H, Guenther C, et al. Mineral formation in joints caused by complete or joint-specific loss of ANK function. J Bone Miner Res. 2006;21(8):1238–47.

17. McKee MD, Nanci A. Osteopontin and the bone remodeling sequence. Colloidal-gold immunocytochemistry of an interfacial extracellular matrix protein. Ann NY Acad Sci. 1995;760:177–89.

18. Boskey AL, Spevak L, Paschalis E, Doty SB, McKee MD. Osteopontin deficiency increases mineral content and mineral crystallinity in mouse bone. Calcif Tissue Int. 2002;71(2):145–54.

19. Wronski TJ, Halloran BP, Bikle DD, Globus RK, Morey-Holton ER. Chronic administration of 1,25-dihydroxyvitamin D3: increased bone but impaired mineralization. Endocrinology. 1986;119(6): 2580–5.

20. Erben RG, Kohn B, Weiser H, Sinowatz F, Rambeck WA. Role of vitamin D metabolites in the prevention of the osteopenia induced by ovariectomy in the axial and appendicular skeleton of the rat. Z Ernahrungswiss. 1990;29(4):229–48.

21. Lanske B, Razzaque MS. Premature aging in Klotho mutant mice: cause or consequence? Ageing Res Rev. 2007;6(1):73–9.

22. Li YC, Amling M, Pirro AE, et al. Normalization of mineral ion homeostasis by dietary means prevents hyperparathyroidism, rickets, and osteomalacia, but not alopecia in vitamin D receptor-ablated mice. Endocrinology. 1998;139(10):4391–6.

23. Erben RG, Soegiarto DW, Weber K, et al. Deletion of deoxyribonucleic acid binding domain of the vitamin D receptor abrogates genomic and nongenomic functions of vitamin D. Mol Endocrinol. 2002;16(7):1524–37.

24. Schneider MR, Dahlhoff M, Andrukhova O, et al. Normal epidermal growth factor receptor signaling is dispensable for bone anabolic effects of parathyroid hormone. Bone. 2012;50(1):237–44.

25. Bouxsein ML, Boyd SK, Christiansen BA, Guldberg RE, Jepsen KJ, Muller R. Guidelines for assessment of bone microstructure in rodents using micro-computed tomography. J Bone Miner Res. 2010;25(7):1468–86.

26. Roschger P, Paschalis EP, Fratzl P, Klaushofer K. Bone mineralization density distribution in health and disease. Bone. 2008;42(3):456–66.

27. Erben RG. Embedding of bone samples in methylmethacrylate: an improved method suitable for bone histomorphometry, histochemistry, and immunohistochemistry. J Histochem Cytochem. 1997;45(2):307–13.

28. Schenk R. Preparation of calcified tissues for light microscopy. Methods Calcif Tissue Prep. 1984;1:1–56.

29. Jiang X, Ye M, Jiang X, et al. Method development of efficient protein extraction in bone tissue for proteome analysis. J Proteome Res. 2007;6(6):2287–94.

30. Shimada T, Kakitani M, Yamazaki Y, et al. Targeted ablation of Fgf23 demonstrates an essential physiological role of FGF23 in phosphate and vitamin D metabolism. J Clin Invest. 2004;113(4): 561–8.

31. Jones G, Prosser DE, Kaufmann M. 25-Hydroxyvitamin D-24-hydroxylase (CYP24A1): its important role in the degradation of vitamin D. Arch Biochem Biophys. 2012;523(1):9–18.

32. Takeyama K, Kitanaka S, Sato T, Kobori M, Yanagisawa J, Kato S. 25-Hydroxyvitamin D3 1alpha-hydroxylase and vitamin D synthesis. Science. 1997;277(5333):1827–30.

33. Mackenzie NC, Zhu D, Milne EM, et al. Altered bone development and an increase in FGF-23 expression in Enpp1(-/-) mice. PLoS One. 2012;7(2):e32177.

34. Ho AM, Johnson MD, Kingsley DM. Role of the mouse ank gene in control of tissue calcification and arthritis. Science. 2000;289(5477): 265–70.

35. Murshed M, Harmey D, Millan JL, McKee MD, Karsenty G. Unique coexpression in osteoblasts of broadly expressed genes accounts for the spatial restriction of ECM mineralization to bone. Genes Dev. 2005;19(9):1093–104.

36. Bellows CG, Heersche JN, Aubin JE. Inorganic phosphate added exogenously or released from beta-glycerophosphate initiates mineralization of osteoid nodules in vitro. Bone Miner. 1992;17(1): 15–29.

37. Beck GR Jr, Moran E, Knecht N. Inorganic phosphate regulates multiple genes during osteoblast differentiation, including Nrf2. Exp Cell Res. 2003;288(2):288–300.

38. Fatherazi S, Matsa-Dunn D, Foster BL, Rutherford RB, Somerman MJ, Presland RB. Phosphate regulates osteopontin gene transcription. J Dent Res. 2009;88(1):39–44.

39. Beck GR Jr, Zerler B, Moran E. Phosphate is a specific signal for induction of osteopontin gene expression. Proc Natl Acad Sci USA. 2000;97(15):8352–7.

40. Beck GR Jr, Knecht N. Osteopontin regulation by inorganic phosphate is ERK1/2-, protein kinase C-, and proteasome-dependent. J Biol Chem. 2003;278(43):41921–9.

41. Addison WN, Azari F, Sorensen ES, Kaartinen MT, McKee MD. Pyrophosphate inhibits mineralization of osteoblast cultures by binding to mineral, up-regulating osteopontin, and inhibiting alkaline phosphatase activity. J Biol Chem. 2007;282(21): 15872–83.

42. Harmey D, Hessle L, Narisawa S, Johnson KA, Terkeltaub R, Millan JL. Concerted regulation of inorganic pyrophosphate and osteopontin by akp2, enpp1, and ank: an integrated model of the pathogenesis of mineralization disorders. Am J Pathol. 2004;164(4):1199–209.

43. Kawai M, Kinoshita S, Kimoto A, et al. FGF23 suppresses chondrocyte proliferation in the presence of soluble alpha-Klotho both in vitro and in vivo. J Biol Chem. 2013;288(4):2414–27.

44. Hessle L, Johnson KA, Anderson HC, et al. Tissue-nonspecific alkaline phosphatase and plasma cell membrane glycoprotein-1 are central antagonistic regulators of bone mineralization. Proc Natl Acad Sci USA. 2002;99(14):9445–9.

45. Wennberg C, Hessle L, Lundberg P, et al. Functional characterization of osteoblasts and osteoclasts from alkaline phosphatase knockout mice. J Bone Miner Res. 2000;15(10):1879–88.

46. Narisawa S, Yadav MC, Millan JL. In vivo overexpression of tissue-nonspecific alkaline phosphatase increases skeletal mineralization and affects the phosphorylation status of osteopontin. J Bone Miner Res. 2013;28(7):1587–98.

47. Barros NM, Hoac B, Neves RL, et al. Proteolytic processing of osteopontin by PHEX and accumulation of osteopontin fragments in Hyp mouse bone, the murine model of X-linked hypophosphatemia. J Bone Miner Res. 2013;28(3):688–99.

48. Martin A, Liu S, David V, et al. Bone proteins PHEX and DMP1 regulate fibroblastic growth factor Fgf23 expression in osteocytes through a common pathway involving FGF receptor (FGFR) signaling. FASEB J. 2011;25(8):2551–62.